



LAWRENCE
LIVERMORE
NATIONAL
LABORATORY

Plasma Collision in a Gas Atmosphere

S. Le Pape, L. Divol, G. Huser, J. Katz, A. Kemp, J. S.
Ross, S. Wallace, S. Wilks

February 28, 2023

Physics Review Letters

Disclaimer

This document was prepared as an account of work sponsored by an agency of the United States government. Neither the United States government nor Lawrence Livermore National Security, LLC, nor any of their employees makes any warranty, expressed or implied, or assumes any legal liability or responsibility for the accuracy, completeness, or usefulness of any information, apparatus, product, or process disclosed, or represents that its use would not infringe privately owned rights. Reference herein to any specific commercial product, process, or service by trade name, trademark, manufacturer, or otherwise does not necessarily constitute or imply its endorsement, recommendation, or favoring by the United States government or Lawrence Livermore National Security, LLC. The views and opinions of authors expressed herein do not necessarily state or reflect those of the United States government or Lawrence Livermore National Security, LLC, and shall not be used for advertising or product endorsement purposes.

Plasma collision in a gas atmosphere

S. Le Pape,¹ L. Divol,¹ G. Huser,² J. Katz,³ A. Kemp,¹ J.S. Ross,¹ S. Wallace,¹ and S. Wilks¹

¹*Lawrence Livermore National Laboratory, Livermore, CA 94550, USA*

²*CEA, DAM, DIF, Bruyeres-le-Chatel, F-91297 Arpajon, France*

³*Laboratory for Laser Energetics, University of Rochester,
250 East River Road, Rochester, New York 14623, USA*

(Dated: March 26, 2019)

We present a study on the impact of a gas atmosphere on the collision of two counter propagating plasmas (gold and carbon). Imaging optical Thomson scattering data of the plasma collision with and without helium in between have been obtained on the Omega laser facility. We observed the presence of gold ions across the entire field of view in the vacuum case. Once Helium is added, the two plasmas remain separated. The dramatic difference in ionic temperature is consistent with a reduction of the maximum flow velocity from $M=7$ to $M=4$ due to the presence of helium. The presence a small amount of helium is enough to transition from an interpenetrating regime to a regime in better agreement with a hydrodynamic description of the system.

PACS numbers: 52.50.Jm, 52.25.Os, 52.27.Gr, 52.65.Yy

Plasma collisions are present in a large range of conditions which impact the characteristics of the collision. At low-density, plasma collision can lead to the formation of collisionless shocks [1],[2] that are thought to be the source of magnetic fields and particle acceleration to cosmic ray energies. At higher ion density, it can lead to the formation of a hot dense plasma used to generate X-ray lasers [3]. Colliding plasma are also a key feature in fusion chambers where the chamber walls are exposed to extreme flux that are expected to generate stagnation of plasma clouds that could limit the lifetime of fusion chambers [4], [5]. In Inertial Confinement Fusion (ICF), inside a hohlraum the ablated gold can stagnate on the ablated low density plasma from the capsule leading to impaired propagation on the laser beams [6].

Stagnation from the hohlraum walls has been prevented in ICF plasma by adding up to 1.6 mg/cm^{-3} of helium in hohlraums [7], due to the helium back pressure on the expanding gold. But the presence of helium is not without negative impact on the hohlraum performance [8],[9],[10]. Lowering the helium density (down to 0.03 mg/cm^{-3}), enabled by the use of shorter laser pulses, has been a successful strategy to increase laser to hohlraum coupling and reduce Laser Plasma Interaction (LPI) [11],[12]. It has also revealed a surprising transition in plasma conditions, going from 0.3 to 0.03 mg/cm^{-3} of helium density. At 0.3 mg/cm^{-3} , radiation hydrodynamic simulations are a good description of the plasma conditions and energy deposition inside the hohlraum [13],[14]. At 0.03 mg/cm^{-3} , the same model does not reflect the changes in plasma conditions implied by the changes in the energy spatial repartition inside the hohlraum [15]. Indirect observable have shown that kinetic effects might apply in the near vacuum case. In a reduced scale vacuum hohlraum on Omega, a gold wall-gas diffusion layer have been observed using proton radiography [16] suggesting gold mixing into the helium gas,

DD ions accelerated by an electrostatic shock formed in the gold/carbon mix layer have been observed in vacuum hohlraums [17] but no direct measurement of the plasma conditions have been made so far.

In this paper, we have studied the impact of adding helium gas on the collision of two laser driven plasmas using imaging optical Thomson Scattering. Adding 0.15 mg/cc of helium, a density equals to 0.5% of the critical density at 3ω , has a dramatic effect on the plasma collision. In the absence of helium (vacuum case), gold ions can be observed to travel up to hundreds of microns in the ablated carbon. Adding helium, the mixed zone is reduced to $\sim 50 \mu\text{m}$. The plasma conditions resulting from the collision are also greatly different; the vacuum case result in a hot (tens of keV) mixed plasma, when the case with helium result in a $< 2 \text{ keV}$ plasma. The presence of ambient helium between the two plasma limits the peak velocity reached by the gold ions, reducing their peak velocities from a Mach number $M = 7$ in vacuum to ~ 4 when helium is present. This reduction of a factor 1.75 in peak velocity implies a reduction by a factor of ~ 10 of the mean free path of gold ions into ablated carbon.

An experiment was carried out on the Omega laser facility [18] to measure the plasma conditions using Optical Thomson Scattering in a relevant reduced scale experiment. Nineteen, $\lambda_{3\omega}=351\text{-nm}$, laser beams were focused using $300 \mu\text{m}$ phase plates on the inside of a gold ring to produce a gold blow-off plasma. Nine beams were focused onto a High Density Carbon (HDC) ring inside the gold ring to produce carbon blow-off plasma with flow velocities relevant to the NIF conditions, the two rings are separated by a 1-mm gap (figure 1-a). To study the impact of Helium on plasma conditions, the two ring/rod were placed inside a gas bag filled with $\sim 0.15 \text{ mg/cc}$ of He4. For the vacuum shot, i.e no gas bag, each beam had 300 J in a 1-ns flat top pulse (figure 1-c). When a gas bag was used each beam has $\sim 370 \text{ J}$ in a stepped pulse with

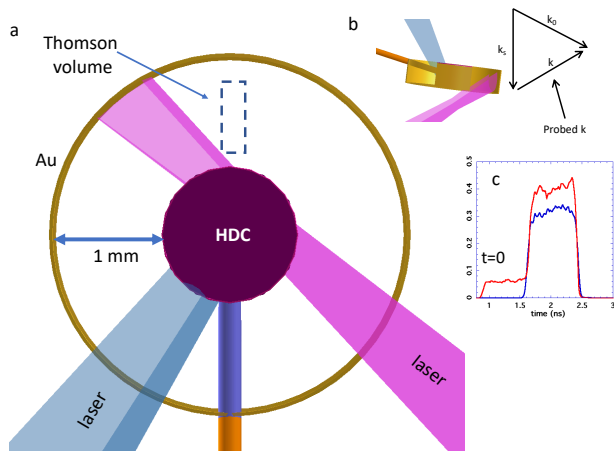


FIG. 1. a) Schematic of the target for the Gold/Carbon case, the blue rectangle represents where the area where the Thomson measurement is made. b) Geometry of the Thomson probe. c) blue: laser pulse shape used without the helium gas bag, red: laser pulse shape used with the helium gas bag.

300 J in a 1-ns flat top pulse. The Thomson-scattering diagnostic [19] consisted of a 40-J, 1-ns-long, $\lambda_{4\omega}=263.23$ -nm probe beam with a best-focus diameter of $\sim 50\mu\text{m}$ [20]. The light scattered from a $60\mu\text{m} \times 60\mu\text{m} \times 1000\mu\text{m}$ volume was imaged through a 1/3-m spectrometer onto a CCD camera. The spectral dispersion was 0.411 nm/pxl, the scattering angle 60 degree (figure 1-b). The Thomson scattering data is taken at the end on the main laser pulse (figure 1-c) for a ~ 300 ps duration.

Spatially resolved Thomson scattering (TS) spectra are shown on the figure 2-a for the gold/carbon case and figure 2-e for the gold/helium/carbon case. Figures 2-b,c,d and 2-f,g,h show line-outs for the two cases. The flow velocity can be measured from the Doppler shift of the midpoint of the Thomson scattered signal, $\Delta\omega = \omega_a + k_a \cdot v_f$, where v_f is the flow velocity. The velocities of the carbon and gold flow have opposite directions [21] (figure 4-b) leading to red-shifted or blue-shifted spectra. The wavelength separation of the two ionic peak is roughly proportional to $\sqrt{\frac{ZT_e + 3T_i}{M_i}}$, we assumed fully ionized carbon $Z=6$ and $Z=45$ for gold. The ionic peak separation allows the determination of the electron temperature (T_e) when $\frac{T_i}{ZT_e}$ is small. Ionic Landau damping, when $\frac{T_i}{ZT_e}$ is sizable, broadens the ionic peak enabling the determination of the ion temperature. Throughout this paper the TS spectra are fitted using a multi-species, multi-flow kinetic model for the plasma dispersion, which usually allows a determination of the temperature and average flow velocity for each species.

In the vacuum case, the entire plasma at the time of the measurement is a hot mix of Au and C ions, the two

counter-streaming plasmas having interpenetrated (Fig. 2-a). When a low density (0.15 mg/cc) ambient Helium gas is added, a narrow ($\sim 50\mu\text{m}$) cold mix layer separate the Au plasma from the Carbon plasma (Fig. 2-e), with the He ions diffusing across the boundary. From the line-outs on figure 2 more detailed data on the plasma conditions can be extracted. At the $200\mu\text{m}$ position (figure 2-b,f), ion gold peaks are observed in both cases. In the gold/carbon case, a blue-shifted tail and an asymmetry of the ionic peak can be observed. The blue-shifted tail and peak asymmetry is indicative of fast carbon ions having reached this position. In the gold/helium/carbon case, only one gold peak is observed. The presence of light helium ions is responsible of the Landau damping of the gold ion wave [22],[23]. A similar effect is observed in the carbon/gold case but the plasma conditions are such that it leads only to an asymmetry of the gold ion peaks. At the $400\mu\text{m}$ position (figure 2 c,g), the gold/carbon case shows a broad single peak while the gold/helium/carbon case shows two separated carbon peaks. The broad ionic peak observed is due to the presence of hot ($> 20\text{keV}$) gold and carbon ions in the same region. The two asymmetric carbon ion peaks observed are due to the presence of cold ($< 1\text{keV}$) carbon mixed with cold ($< 1\text{keV}$) helium ion. At the $650\mu\text{m}$ position (figure 2 d,h), in the gold/carbon case, two carbon peaks are observed with a blue-shifted tail indicative of the presence of fast gold ions. At the same position in the gold/helium/carbon case, no tail is observed with almost symmetric Carbon peaks, indicative of a pure C plasma with a trace of He.

From similar fits at various positions along the space axis, the temperature (ion and electron) and species fraction profile can be inferred (figure 3). Figure 3-a-b shows the ion species fraction for the two cases, where the transition from a sharp separation of the two fluids by a narrow mixing layer when ambient He is added to a uniformly hot mixed plasma in the vacuum case is clear. In the Au/C case, gold is present throughout the field of view, at a fraction ranging from 5×10^{-2} , $200\mu\text{m}$ away from the gold wall to $\sim 10^{-3}$, $300\mu\text{m}$ away from the carbon puck. In the Au/He/C case, gold is only present in the first $300\mu\text{m}$ from the gold wall, along with helium at about 50/50 ratio. From $350\mu\text{m}$ to the carbon puck, only carbon and helium are present, with a helium fraction ranging from 0.5 to about zero next to the carbon puck. Figure 3-c,d show the temperature profile for the two cases. In the Au/C case the ion temperature of the carbon is ~ 20 keV where the gold species fraction is above 10^{-3} , while it stays below 1 keV everywhere when ambient He is added. Very close to the carbon puck, the carbon temperature is similar in both cases, around 1 keV, as the ablation physics is dominated by laser absorption.

Time resolved data (the scattered signal is imaged onto a optical streak camera) at the $400\mu\text{m}$ spatial position are shown on figure 4 for the Au/C case using the same

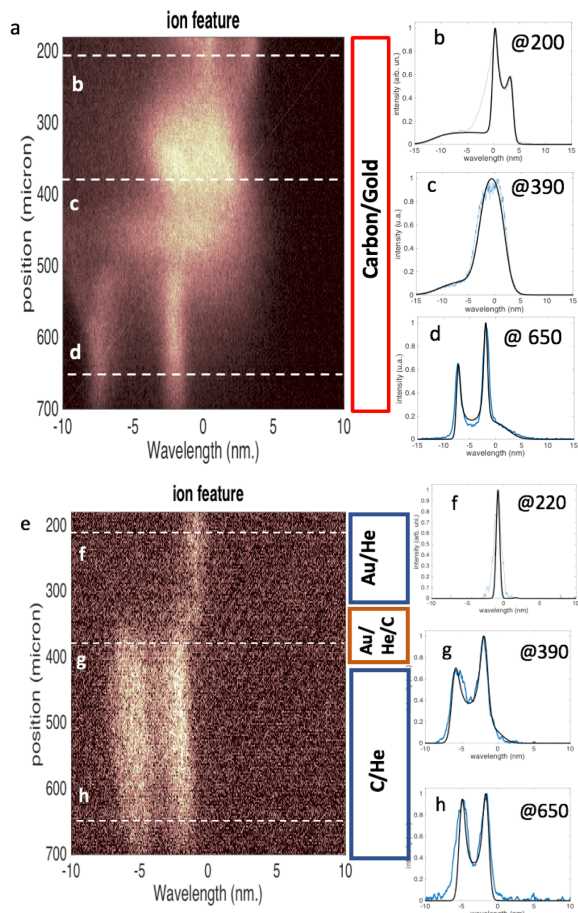


FIG. 2. a) Spatially resolved Thomson scattering spectra in the Gold/Carbon case. b,c,d) blue curves: Line outs over figure 2-a at various positions along the spatial axis. Black curve: theoretical fits to experimental data f) Spatially resolved Thomson scattering spectra in the Gold/helium Carbon case. f,g,h) blue curves: Line outs over figure 2-e at various positions along the spatial axis. Black curve: theoretical fits to experimental data

laser drive (300J per laser beam). The Thomson probe was on for 1 ns, starting 300 ps after the beginning of the main laser driver. Figure 4-b shows that the flow velocities of the two species decrease in time as the ion temperature of the two species increases (figure 4-a) implying a transfer from the kinetic energy of the counter-streaming flows into thermal energy through Coulomb collisions[24]. Time resolved and spatially resolved data are in good agreement (spatial data are taken at 1 ns for 300 ps). Carbon ion temperature is already at $\sim 10keV$ at 0.9 ns which is within a factor of two of the ion temperature measured at the same location later in time. Figure 4-c shows the ion concentration of the two species as a function of time. At 300 ps the gold and carbon are already mixed, which explained the high gold ion temperature ($\sim 20keV$). By 600 ps, the gold starts to push the carbon away from the probed zone leading to a de-

crease of the carbon ion density (figure 4-c). At all times the plasma is mostly composed of carbon ions with a small fraction ($< 1\%$) of Au ions, similar to the late-time spatially resolved data at this probed position.

The large differences in ion temperature reached for the two cases (tens of keV for the Au/C case, $\sim 1keV$ for the Au/He/C), in mix layer width and composition can be explained by the strong slowdown of the front of a plasma expansion in vacuum in the presence of a low density ambient plasma. For the Au/C case, the early laser driven expansion of the gold (and carbon) can be approximated by a self-similar isothermal expansion [25] for the electron density $N_e = N_0 * \exp(-(\xi + 1))$ and flow velocity $v_i = C_s(\xi + 1)$, where $\xi = \frac{x}{C_s t}$, N_0 is the critical density for a 32 degree angle of incidence and $C_s = \sqrt{\frac{\gamma Z K_b T_e}{M_i}}$ is the ion sound speed (here the ion sound speed is calculated for $T_e = 1keV$, $Z=45$ for gold ions of fig 4.a, $C_s \sim 1.9 \times 10^7 cm/s$). In a self-similar description, the flow velocity increases indefinitely with time and space. This description breaks down when the Debye length equals the density scale length $C_s t$ [26] due to charge separation effects. The maximum ion front velocity is then given by [27] $v_{front} = 2C_s \ln(2\tau)$, where $\tau = \frac{\omega_{pi} t}{\sqrt{2e}}$, ω_{pi} being the ion plasma frequency at N_0 ; at 300 ps we calculate $\tau = 7.5 \times 10^3$ which gives a peak velocity of the gold ions $v_{front} \sim 3.6 \times 10^8 cm/s$, a Mach number $M \sim 19$. The electron density at $M=19$ following the same description is $\sim 3.5 \times 10^{13}$, well below the detection threshold of our diagnostic. Experimentally, from the data shown on figure 4-c, the fastest detected gold ions have reached the Thomson volume located $400\mu m$ from their initial position is 300ps. It corresponds to a velocity of $\sim 1.3 \times 10^8 cm/s$, which is about $M=7$ at a measured electron density of $2 \times 10^{19} cm^{-3}$, which is higher than the density inferred from the self-similar expansion at $M=7$ ($n_e \sim 6 \times 10^{18}$). Figure 4-a shows that the ion temperature at 300ps is already high ($> 2keV$), suggesting that the gold ions have already slowed down on the carbon leading to a higher ion density.

In the Gold/Helium/Carbon case, the ion front velocity is not limited by space charge effects but by the density of the helium at the Gold/Helium interface [28]. This interface is a contact discontinuity, where pressure and velocity are continuous. The laser will maintain a continuous electron temperature. Assuming fully ionized He, $Z = 45$ for Au and $T_{Au} \sim T_{He} \sim T_e$ near the interface as measured (Fig.3-d), equating pressures $P = N_e(T_e + T_i/Z)$ on both sides leads to $N_e(Au) = 3/2N_e(He)$. Laser-heated Helium is weakly shocked by the Au expansion, and one can finally assume for this estimate that $N_e(Au) \sim 1 \times 10^{20} cm^{-3}$, roughly twice the initial gas density.

Less than 1% helium density is transparent for the laser, one can then assume that the self-similar expansion is comparable for both the helium and the vacuum

case. The peak gold ion velocity, set by the helium density at the Au/He interface, would have then a Mach number $\sim M = 4$, much less than in the vacuum case.

This difference in peak velocity of the gold ions has a significant impact on the mean free path on the gold ions in Carbon. The ion-ion mean free path of a supersonic flow into a counter propagating flow scales as v^4 where v is the relative velocity of the two flows[29]. From the vacuum to the helium case, the velocity of the gold flow decreases by a factor 1.75 which is a factor of ~ 10 in mean free path. From the conditions measured at 300 ps in the vacuum case (cf fig 4), the relative flow velocity is $\sim 10^8 \text{ cm/s}$, the ion density is $\sim 5 \times 10^{19} \text{ cm}^{-3}$, the mean free path of a gold ion into carbon is about $\sim 500 \mu\text{m}$.

The impact of the presence of gold or helium ions mixed with the ablated carbon is also significant knowing that in a hohlraum laser beams mostly propagate through ablated carbon. The Inverse-Bremstrahlung coefficient for a multi species plasma follows: $\kappa \propto \frac{n_e^2 Z_{eff}}{T_e^{3/2}}$ where $Z_{eff} = \frac{\bar{Z}^2}{\bar{Z}}$ where $\bar{Z}^2 = \sum_j Z_j^2 f_j$ [30] and $f_i \equiv \frac{n_j}{N_i}$. For the plasma conditions described on figure 4, where the gold ion represents 2% of the total ion population, the effective charge state goes from 6 for a pure carbon plasma fully ionized to ~ 14 in the gold/carbon case. This results in an increase by a factor of 3 of the Inverse-Bremstrahlung coefficient in the mixed case assuming the same electron density and electron temperature. The higher initial laser absorption in the mixed gold carbon region than in the carbon/helium did result in an higher electron temperature (figure 3-c,d), but as the electron temperature increases the plasma becomes more transparent, assuming an isobaric condition where an increase in temperature would result in a decrease in electron density. The electron-ion equilibration time is the order of $\sim 10 \text{ ns}$ in these conditions is too long to explain the higher measured electron temperature.

This experiment was designed to emulate at reduced scale plasma conditions of a NIF hohlraum. The laser intensity on the wall of the Omega target is in the same range (low 10^{14} W/cm^2) as the intensity reached on the NIF. We can now explain the surprising transition observed on the NIF when the helium density was lowered below 0.3 mg/cc . In the vacuum case, gold and carbon are fully mixed when the slowdown of the gold and carbon ions caused by 0.15 mg/cc of helium prevents gold from mixing into the carbon plasma. These changes in plasma conditions with helium density can explain the disagreement between Radiation-hydrodynamic simulations [31] and experimental data [32] observed in the vacuum case and the overall good agreement at 0.3 mg/cc [33],[13].

In conclusion, we report on a direct measurement of the impact of a gas atmosphere on the collision of two counter-propagating plasmas. Spatially and time resolved Optical Thomson scattering data show that the presence of helium, by limiting the peak velocity achieved

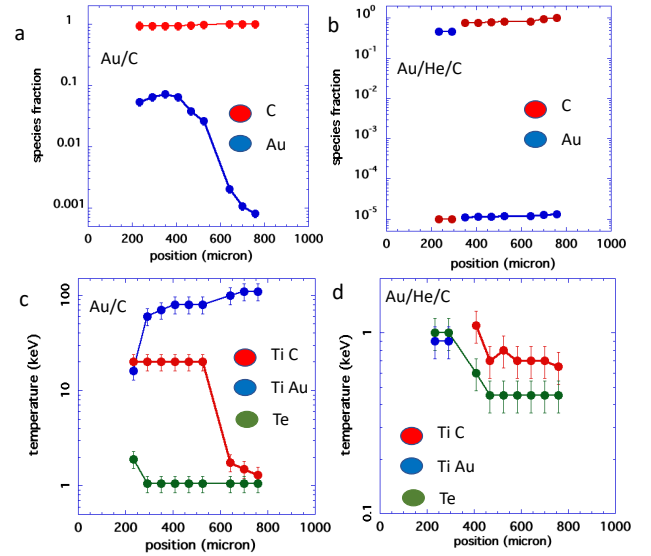


FIG. 3. Zero is the initial position of the gold ring, thousand is the initial position of the carbon puck for all four plots. a) species fraction for the gold/carbon case as a function of space. b) species fraction for the gold/helium/carbon case as a function of space. c) Temperature (ion and electron) the gold/carbon case as a function of space. d) Temperature (ion and electron) the gold/helium/carbon case as a function of space.

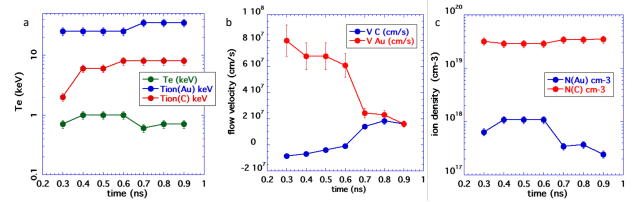


FIG. 4. all three plots are for the gold/carbon case. a) Temperature (ion and electron) as a function of time. b) Flow velocities as a function of time. c) Ion density as a function of time.

by the gold ions, prevents gold from mixing into the ablated carbon. The impact of gold ions interpenetrating into the ablated carbon on plasma conditions is significant: the ion temperatures measured (gold or carbon) are in the 10's of keV when it is less than 2 keV for the Carbon/helium/gold case. The possibility of controlling the intensity of the collision by adding a small density of ambient gas is a key feature in environments such as fusion reactors or ICF hohlraums.

This work was performed under the auspices of the U.S. Department of Energy by Lawrence Livermore National Laboratory under Contract DE-AC52-07NA27344. Work was also supported by the Laboratory Directed Research and Development Grant 11-ERD-050 and the National Laboratory User Facility and by General Atomics under Contract DE-NA0001808.

-
- [1] H. Takabe, T. N. Kato, Y. Sakawa, Y. Kuramitsu, T. Morita, T. Kadono, K. Shigemori, K. Otani, H. Nagatomo, T. Norimatsu, et al., *Plasma Physics and Controlled Fusion* **50**, 124057 (2008), URL <http://stacks.iop.org/0741-3335/50/i=12/a=124057>.
- [2] C. M. Huntington, F. Fiuza, J. S. Ross, A. B. Zylstra, R. P. Drake, D. H. Froula, G. Gregori, N. L. Kugland, C. C. Kuranz, M. C. Levy, et al., *Nature Physics* **11**, 173 EP (2015), URL <http://dx.doi.org/10.1038/nphys3178>.
- [3] T. Boehly, B. Yaakobi, D. Shvarts, D. Meyerhofer, P. Audebert, J. Wang, M. Russotto, B. Boswell, R. Epstein, R. S. Craxton, et al., *Applied Physics B* **50**, 165 (1990), ISSN 1432-0649, URL <https://doi.org/10.1007/BF00357279>.
- [4] K. F. Al-Shboul, S. S. Harilal, S. M. Hassan, A. Hassanein, J. T. Costello, T. Yabuuchi, K. A. Tanaka, and Y. Hirooka, *Physics of Plasmas* **21**, 013502 (2014), <https://doi.org/10.1063/1.4859136>, URL <https://doi.org/10.1063/1.4859136>.
- [5] Y. Hirooka, T. Oishi, H. Sato, and K. A. Tanaka, *Fusion Science and Technology* **60**, 804 (2011), <https://doi.org/10.13182/FST11-A12484>, URL <https://doi.org/10.13182/FST11-A12484>.
- [6] P. W. Rambo and J. Denavit, *Physics of Plasmas* **1**, 4050 (1994), <https://doi.org/10.1063/1.870875>, URL <https://doi.org/10.1063/1.870875>.
- [7] G. Huser, C. Courtois, and M.-C. Monteil, *Physics of Plasmas* **16**, 032703 (2009), <https://doi.org/10.1063/1.3099054>, URL <https://doi.org/10.1063/1.3099054>.
- [8] D. E. Hinkel, L. F. Berzak Hopkins, T. Ma, J. E. Ralph, F. Albert, L. R. Benedetti, P. M. Celliers, T. Döppner, C. S. Goyon, N. Izumi, et al., *Phys. Rev. Lett.* **117**, 225002 (2016), URL <https://link.aps.org/doi/10.1103/PhysRevLett.117.225002>.
- [9] O. S. Jones, C. J. Cerjan, M. M. Marinak, J. L. Milovich, H. F. Robey, P. T. Springer, L. R. Benedetti, D. L. Bleuel, E. J. Bond, D. K. Bradley, et al., *Physics of Plasmas* **19**, 056315 (2012), <https://doi.org/10.1063/1.4718595>, URL <https://doi.org/10.1063/1.4718595>.
- [10] A. L. Kritcher, D. E. Hinkel, D. A. Callahan, O. A. Hurricane, D. Clark, D. T. Casey, E. L. Dewald, T. R. Dittrich, T. Doppner, M. A. B. Garcia, et al., *Physics of Plasmas* **23**, 052709 (2016).
- [11] L. F. Berzak Hopkins, N. B. Meezan, S. Le Pape, L. Divol, A. J. Mackinnon, D. D. Ho, M. Hohenberger, O. S. Jones, G. Kyrala, J. L. Milovich, et al., *Phys. Rev. Lett.* **114**, 175001 (2015), URL <https://link.aps.org/doi/10.1103/PhysRevLett.114.175001>.
- [12] S. Le Pape, L. Divol, L. Berzak Hopkins, A. Mackinnon, N. B. Meezan, D. Casey, J. Frenje, H. Herrmann, J. McNaney, T. Ma, et al., *Phys. Rev. Lett.* **112**, 225002 (2014), URL <https://link.aps.org/doi/10.1103/PhysRevLett.112.225002>.
- [13] L. B. Hopkins, S. LePape, L. Divol, A. Pak, E. Dewald, D. D. Ho, N. Meezan, S. Bhandarkar, L. R. Benedetti, T. Bunn, et al., *Plasma Physics and Controlled Fusion* **61**, 014023 (2018), URL <https://doi.org/10.1088/2F1361-6587/2Faad97e>.
- [14] K. L. Baker, C. A. Thomas, D. T. Casey, S. Khan, B. K. Spears, R. Nora, T. Woods, J. L. Milovich, R. L. Berger, D. Strozzi, et al., *Phys. Rev. Lett.* **121**, 135001 (2018), URL <https://link.aps.org/doi/10.1103/PhysRevLett.121.135001>.
- [15] L. F. Berzak Hopkins, S. Le Pape, L. Divol, N. B. Meezan, A. J. Mackinnon, D. D. Ho, O. S. Jones, S. Khan, J. L. Milovich, J. S. Ross, et al., *Physics of Plasmas* **22**, 056318 (2015), <https://aip.scitation.org/doi/pdf/10.1063/1.4921151>, URL <https://aip.scitation.org/doi/abs/10.1063/1.4921151>.
- [16] C. K. Li, F. H. Séguin, J. A. Frenje, M. Rosenberg, R. D. Petrasso, P. A. Amendt, J. A. Koch, O. L. Landen, H. S. Park, H. F. Robey, et al., *Science* **327**, 1231 (2010), ISSN 0036-8075, <https://science.sciencemag.org/content/327/5970/1231.full.pdf>, URL <http://science.sciencemag.org/content/327/5970/1231>.
- [17] L. Q. Shan, H. B. Cai, W. S. Zhang, Q. Tang, F. Zhang, Z. F. Song, B. Bi, F. J. Ge, J. B. Chen, D. X. Liu, et al., *Phys. Rev. Lett.* **120**, 195001 (2018), URL <https://link.aps.org/doi/10.1103/PhysRevLett.120.195001>.
- [18] T. R. Boehly, R. S. Craxton, T. H. Hinterman, P. A. Jaanimagi, J. H. Kelly, T. J. Kessler, R. L. KREMENS, S. A. Kumpan, S. A. Letzring, R. L. McCrory, et al., *Fusion Technology* **26**, 722 (1994).
- [19] J. Katz, R. Boni, C. Sorce, R. Follett, M. J. Shoup, and D. H. Froula, *Review of Scientific Instruments* **83**, 10E349 (2012), <https://doi.org/10.1063/1.4733551>, URL <https://doi.org/10.1063/1.4733551>.
- [20] A. J. Mackinnon, S. Shiromizu, G. Antonini, J. Auerbach, K. Haney, D. H. Froula, J. Moody, G. Gregori, C. Constantin, C. Sorce, et al., *Review of Scientific Instruments* **75**, 3906 (2004), <https://doi.org/10.1063/1.1789247>, URL <https://doi.org/10.1063/1.1789247>.
- [21] R. K. Follett, J. A. Delettrez, D. H. Edgell, R. J. Henchen, J. Katz, J. F. Myatt, and D. H. Froula, *Review of Scientific Instruments* **87**, 11E401 (2016), <https://aip.scitation.org/doi/pdf/10.1063/1.4959160>, URL <https://aip.scitation.org/doi/abs/10.1063/1.4959160>.
- [22] P. Neumayer, R. L. Berger, L. Divol, D. H. Froula, R. A. London, B. J. MacGowan, N. B. Meezan, J. S. Ross, C. Sorce, L. J. Suter, et al., *Phys. Rev. Lett.* **100**, 105001 (2008), URL <https://link.aps.org/doi/10.1103/PhysRevLett.100.105001>.
- [23] S. H. Glenzer, C. A. Back, K. G. Estabrook, R. Wallace, K. Baker, B. J. MacGowan, B. A. Hammel, R. E. Cid, and J. S. De Groot, *Phys. Rev. Lett.* **77**, 1496 (1996), URL <https://link.aps.org/doi/10.1103/PhysRevLett.77.1496>.
- [24] C. Chenais-Popovics, P. Renaudin, O. Rancu, F. Gilleron, J.-C. Gauthier, O. Larroche, O. Peyrusse, M. Dirksmiller, P. Sondhauss, T. Missalla, et al., *Physics of Plasmas* **4**, 190 (1997), <https://doi.org/10.1063/1.872132>, URL <https://doi.org/10.1063/1.872132>.
- [25] J. Denavit, *The Physics of Fluids* **22**, 1384 (1979), <https://aip.scitation.org/doi/pdf/10.1063/1.862751>, URL <https://aip.scitation.org/doi/abs/10.1063/1.862751>.
- [26] J. S. Pearlman and R. L. Morse, *Phys. Rev. Lett.*

- 40, 1652 (1978), URL <https://link.aps.org/doi/10.1103/PhysRevLett.40.1652>.
- [27] P. Mora, Phys. Rev. Lett. **90**, 185002 (2003), URL <https://link.aps.org/doi/10.1103/PhysRevLett.90.185002>.
- [28] A. V. GUREVICH, Sov. Phys.-JETP **22**, 449 (1989).
- [29] A. Decoster, P. A. Markowich, B. Perthame, and P.-A. Raviart, *Modeling of collisions*, vol. 2 (Elsevier, 1998).
- [30] D. J. Strozzi, E. A. Williams, D. E. Hinkel, D. H. Froula, R. A. London, and D. A. Callahan, Physics of Plasmas **15**, 102703 (2008), <https://doi.org/10.1063/1.2992522>, URL <https://doi.org/10.1063/1.2992522>.
- [31] M. M. Marinak, G. D. Kerbel, N. A. Gentile, O. Jones, D. Munro, S. Pollaine, T. R. Dittrich, and S. W. Haan, Physics of Plasmas **8**, 2275 (2001).
- [32] L. F. B. Hopkins, S. L. Pape, L. Divol, N. B. Meezan, A. J. Mackinnon, D. D. Ho, O. S. Jones, S. Khan, J. L. Milovich, J. S. Ross, et al., Physics of Plasmas **22**, 056318 (2015).
- [33] D. T. Casey, C. A. Thomas, K. L. Baker, B. K. Spears, M. Hohenberger, S. F. Khan, R. C. Nora, C. R. Weber, D. T. Woods, O. A. Hurricane, et al., Physics of Plasmas **25**, 056308 (2018), <https://doi.org/10.1063/1.5019741>, URL <https://doi.org/10.1063/1.5019741>.